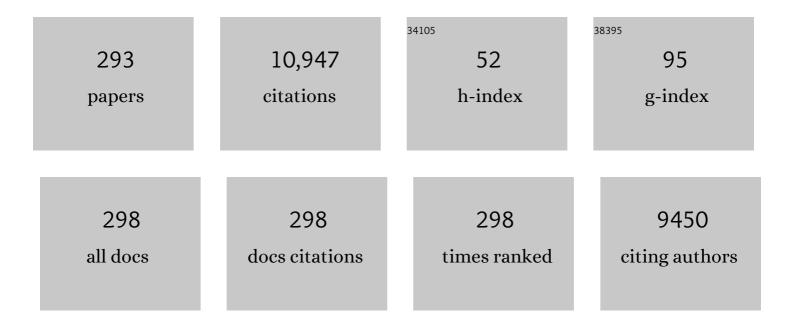
List of Publications by Year in descending order

Source: https://exaly.com/author-pdf/1591422/publications.pdf Version: 2024-02-01



#	Article	IF	CITATIONS
1	Effects of ain buffer layer on crystallographic structure and on electrical and optical properties of GaN and Ga1ⰒxAlxN (0 < x ≦ 0.4) films grown on sapphire substrate by MOVPE. Journal of Crystal Growth, 1989, 98, 209-219.	1.5	689
2	Singleâ€Crystalline ZnS Nanobelts as Ultravioletâ€Light Sensors. Advanced Materials, 2009, 21, 2034-2039.	21.0	537
3	Centimeterâ€Long V ₂ O ₅ Nanowires: From Synthesis to Fieldâ€Emission, Electrochemical, Electrical Transport, and Photoconductive Properties. Advanced Materials, 2010, 22, 2547-2552.	21.0	359
4	Singleâ€Crystalline CdS Nanobelts for Excellent Fieldâ€Emitters and Ultrahigh Quantumâ€Efficiency Photodetectors. Advanced Materials, 2010, 22, 3161-3165.	21.0	342
5	Efficient Assembly of Bridged <i>β</i> â€Ga ₂ O ₃ Nanowires for Solarâ€Blind Photodetection. Advanced Functional Materials, 2010, 20, 3972-3978.	14.9	292
6	Fabrication of High-Quality In ₂ Se ₃ Nanowire Arrays toward High-Performance Visible-Light Photodetectors. ACS Nano, 2010, 4, 1596-1602.	14.6	289
7	Flexible Ultraviolet Photodetectors with Broad Photoresponse Based on Branched ZnSâ€ZnO Heterostructure Nanofilms. Advanced Materials, 2014, 26, 3088-3093.	21.0	251
8	Ultrahighâ€Performance Solarâ€Blind Photodetectors Based on Individual Single rystalline In ₂ Ge ₂ O ₇ Nanobelts. Advanced Materials, 2010, 22, 5145-5149.	21.0	249
9	An Efficient Way to Assemble ZnS Nanobelts as Ultravioletâ€Light Sensors with Enhanced Photocurrent and Stability. Advanced Functional Materials, 2010, 20, 500-508.	14.9	222
10	Highâ€Performance Blue/Ultraviolet‣ightâ€Sensitive ZnSeâ€Nanobelt Photodetectors. Advanced Materials, 2009, 21, 5016-5021.	21.0	217
11	Effects of surface treatments and metal work functions on electrical properties atp-GaN/metal interfaces. Journal of Applied Physics, 1997, 81, 1315-1322.	2.5	213
12	Deep-ultraviolet solar-blind photoconductivity of individual gallium oxide nanobelts. Nanoscale, 2011, 3, 1120.	5.6	210
13	Polarization independent visible color filter comprising an aluminum film with surface-plasmon enhanced transmission through a subwavelength array of holes. Applied Physics Letters, 2011, 98, .	3.3	208
14	Energy bandâ€gap bowing parameter in an AlxGa1â^'xN alloy. Journal of Applied Physics, 1987, 61, 4540-4543.	2.5	194
15	Electrical Transport and Highâ€Performance Photoconductivity in Individual ZrS ₂ Nanobelts. Advanced Materials, 2010, 22, 4151-4156.	21.0	169
16	Extreme dielectric strength in boron doped homoepitaxial diamond. Applied Physics Letters, 2010, 97, .	3.3	160
17	Singleâ€Crystalline Sb ₂ Se ₃ Nanowires for Highâ€Performance Field Emitters and Photodetectors. Advanced Materials, 2010, 22, 4530-4533.	21.0	147
18	Effects of annealing in an oxygen ambient on electrical properties of ohmic contacts to p-type GaN. Journal of Electronic Materials, 1999, 28, 341-346.	2.2	133

#	Article	IF	CITATIONS
19	High-performance metal-semiconductor-metal deep-ultraviolet photodetectors based on homoepitaxial diamond thin film. Applied Physics Letters, 2006, 89, 113509.	3.3	121
20	Low on-resistance diamond field effect transistor with high-k ZrO2 as dielectric. Scientific Reports, 2014, 4, 6395.	3.3	107
21	Effect of AlN Buffer Layer on AlGaN/α-Al2O3Heteroepitaxial Growth by Metalorganic Vapor Phase Epitaxy. Japanese Journal of Applied Physics, 1988, 27, 1156-1161.	1.5	105
22	Normally-off HfO2-gated diamond field effect transistors. Applied Physics Letters, 2013, 103, .	3.3	105
23	WO3 nanowires on carbon papers: electronic transport, improved ultraviolet-light photodetectors and excellent field emitters. Journal of Materials Chemistry, 2011, 21, 6525.	6.7	103
24	Suspended Singleâ€Crystal Diamond Nanowires for Highâ€Performance Nanoelectromechanical Switches. Advanced Materials, 2010, 22, 5393-5397.	21.0	101
25	Single Schottky-barrier photodiode with interdigitated-finger geometry: Application to diamond. Applied Physics Letters, 2007, 90, 123507.	3.3	96
26	Thermally stable visible-blind diamond photodiode using tungsten carbide Schottky contact. Applied Physics Letters, 2005, 87, 022105.	3.3	94
27	Low contact resistance metals for graphene based devices. Diamond and Related Materials, 2012, 24, 171-174.	3.9	94
28	Visible-blind deep-ultraviolet Schottky photodetector with a photocurrent gain based on individual Zn2GeO4 nanowire. Applied Physics Letters, 2010, 97, .	3.3	89
29	Conduction Mechanism of Leakage Current in Ta2 O 5 Films on Si Prepared by LPCVD. Journal of the Electrochemical Society, 1990, 137, 2876-2879.	2.9	84
30	Epitaxial Growth and Properties of Al x Ga1 â^' x  N  by MOVPE. Journal of the Electrochemical S 1986, 133, 1956-1960.	Society,	82
31	Light intensity dependence of photocurrent gain in single-crystal diamond detectors. Physical Review B, 2010, 81, .	3.2	81
32	Band offsets of Al2O3 and HfO2 oxides deposited by atomic layer deposition technique on hydrogenated diamond. Applied Physics Letters, 2012, 101, .	3.3	76
33	Persistent positive and transient absolute negative photoconductivity observed in diamond photodetectors. Physical Review B, 2008, 78, .	3.2	75
34	Solidâ€phase reactions and crystallographic structures in Zr/Si systems. Journal of Applied Physics, 1991, 69, 7050-7056.	2.5	74
35	Edge emission of AlxGa1â^'xN. Solid State Communications, 1986, 60, 509-512.	1.9	73
36	Effects of NiO on electrical properties of NiAu-based ohmic contacts for p-type GaN. Applied Physics Letters, 1999, 75, 4145-4147.	3.3	73

#	Article	IF	CITATIONS
37	Development of Ni/Al and Ni/Ti/Al ohmic contact materials for p-type 4H-SiC. Materials Science and Engineering B: Solid-State Materials for Advanced Technology, 2003, 98, 286-293.	3.5	72
38	Low-leakage p-type diamond Schottky diodes prepared using vacuum ultraviolet light/ozone treatment. Journal of Applied Physics, 2009, 105, .	2.5	71
39	Thermally stable solar-blind diamond UV photodetector. Diamond and Related Materials, 2006, 15, 1962-1966.	3.9	69
40	Homoepitaxial diamond film growth: High purity, high crystalline quality, isotopic enrichment, and single color center formation. Physica Status Solidi (A) Applications and Materials Science, 2015, 212, 2365-2384.	1.8	68
41	Low-resistance Ta/Ti Ohmic contacts for p-type GaN. Applied Physics Letters, 1999, 74, 275-277.	3.3	67
42	Ohmic Contacts for Compound Semiconductors. Critical Reviews in Solid State and Materials Sciences, 1998, 23, 1-60.	12.3	64
43	An Interface Engineered Multicolor Photodetector Based on nâ€Si(111)/TiO ₂ Nanorod Array Heterojunction. Advanced Functional Materials, 2016, 26, 1400-1410.	14.9	64
44	Enhancement-mode hydrogenated diamond metal-oxide-semiconductor field-effect transistors with Y2O3 oxide insulator grown by electron beam evaporator. Applied Physics Letters, 2017, 110, .	3.3	64
45	Enhanced performance of InGaN solar cell by using a super-thin AlN interlayer. Applied Physics Letters, 2011, 99, .	3.3	62
46	High-temperature ultraviolet detection based on InGaN Schottky photodiodes. Applied Physics Letters, 2011, 99, .	3.3	61
47	Interfacial band configuration and electrical properties of LaAlO3/Al2O3/hydrogenated-diamond metal-oxide-semiconductor field effect transistors. Journal of Applied Physics, 2013, 114, .	2.5	60
48	Comprehensive Investigation of Single Crystal Diamond Deep-Ultraviolet Detectors. Japanese Journal of Applied Physics, 2012, 51, 090115.	1.5	60
49	Carrier transport mechanism of Ohmic contact to p-type diamond. Journal of Applied Physics, 1997, 81, 6815-6821.	2.5	59
50	High-performance metal-semiconductor-metal InGaN photodetectors using CaF2 as the insulator. Applied Physics Letters, 2011, 98, 103502.	3.3	56
51	Carbon-Based Materials: Growth, Properties, MEMS/NEMS Technologies, and MEM/NEM Switches. Critical Reviews in Solid State and Materials Sciences, 2011, 36, 66-101.	12.3	55
52	Initial leakage current paths in the vertical-type GaN-on-GaN Schottky barrier diodes. Applied Physics Letters, 2017, 111, .	3.3	55
53	Morphology-tunable In2Se3 nanostructures with enhanced electrical and photoelectrical performances via sulfur doping. Journal of Materials Chemistry, 2010, 20, 6630.	6.7	54
54	Effects of sp2/sp3 bonding ratios on field emission properties of diamond-like carbon films grown by microwave plasma chemical vapor deposition. Diamond and Related Materials, 2002, 11, 1429-1435.	3.9	51

#	Article	IF	CITATIONS
55	Initial Stage of Growth of Ge on (100)Si by Gas Source Molecular Beam Epitaxy Using GeH4. Japanese Journal of Applied Physics, 1989, 28, L690-L693.	1.5	50
56	Doping and interface of homoepitaxial diamond for electronic applications. MRS Bulletin, 2014, 39, 499-503.	3.5	49
57	Logic Circuits With Hydrogenated Diamond Field-Effect Transistors. IEEE Electron Device Letters, 2017, 38, 922-925.	3.9	49
58	Mechanisms of silicon oxidation at low temperatures by microwaveâ€excited O2gas and O2â€N2mixed gas. Journal of Applied Physics, 1990, 67, 2603-2607.	2.5	46
59	Non-destructive detection of killer defects of diamond Schottky barrier diodes. Journal of Applied Physics, 2011, 110, .	2.5	44
60	Low Resistance TiAl Ohmic Contacts with Multi-Layered Structure for p-Type 4H-SiC. Materials Transactions, 2002, 43, 1684-1688.	1.2	43
61	Photovoltaic Schottky ultraviolet detectors fabricated on boron-doped homoepitaxial diamond layer. Applied Physics Letters, 2006, 88, 033504.	3.3	43
62	Comprehensive Investigation of Single Crystal Diamond Deep-Ultraviolet Detectors. Japanese Journal of Applied Physics, 2012, 51, 090115.	1.5	43
63	Electrical characteristics of hydrogen-terminated diamond metal-oxide-semiconductor with atomic layer deposited HfO2 as gate dielectric. Applied Physics Letters, 2013, 102, .	3.3	42
64	Deposition of TiO2/Al2O3 bilayer on hydrogenated diamond for electronic devices: Capacitors, field-effect transistors, and logic inverters. Journal of Applied Physics, 2017, 121, .	2.5	42
65	Electric Field Breakdown of Lateral Schottky Diodes of Diamond. Japanese Journal of Applied Physics, 2007, 46, L196-L198.	1.5	41
66	Integration of high-dielectric constant Ta2O5 oxides on diamond for power devices. Applied Physics Letters, 2012, 101, .	3.3	41
67	Arbitrary Multicolor Photodetection by Hetero-integrated Semiconductor Nanostructures. Scientific Reports, 2013, 3, 2368.	3.3	41
68	A Multilevel Intermediateâ€Band Solar Cell by InGaN/GaN Quantum Dots with a Strainâ€Modulated Structure. Advanced Materials, 2014, 26, 1414-1420.	21.0	40
69	Growth processes in the initial stages of deposition of Ge films on (100) Si surfaces by GeH4 source molecular beam epitaxy. Journal of Crystal Growth, 1990, 99, 254-258.	1.5	39
70	Demonstration of diamond field effect transistors by AlN/diamond heterostructure. Physica Status Solidi - Rapid Research Letters, 2011, 5, 125-127.	2.4	39
71	Energyâ€Efficient Metal–Insulator–Metalâ€&emiconductor Fieldâ€Effect Transistors Based on 2D Carrier Gases. Advanced Electronic Materials, 2019, 5, 1800832.	5.1	39
72	Thermal Stability of Diamond Photodiodes Using Tungsten Carbide as Schottky Contact. Japanese Journal of Applied Physics, 2005, 44, 7832-7838.	1.5	38

#	Article	IF	CITATIONS
73	Bascule nanobridges self-assembled with ZnO nanowires as double Schottky barrier UV switches. Nanotechnology, 2010, 21, 295502.	2.6	38
74	P-Channel InGaN/GaN heterostructure metal-oxide-semiconductor field effect transistor based on polarization-induced two-dimensional hole gas. Scientific Reports, 2016, 6, 23683.	3.3	37
75	Design and fabrication of high-performance diamond triple-gate field-effect transistors. Scientific Reports, 2016, 6, 34757.	3.3	37
76	Highâ€ŧemperature stability of Au/pâ€ŧype diamond Schottky diode. Physica Status Solidi - Rapid Research Letters, 2009, 3, 211-213.	2.4	36
77	Batch production of single-crystal diamond bridges and cantilevers for microelectromechanical systems. Journal of Micromechanics and Microengineering, 2010, 20, 085002.	2.6	36
78	Nearly ideal vertical GaN Schottky barrier diodes with ultralow turn-on voltage and on-resistance. Applied Physics Express, 2017, 10, 051001.	2.4	36
79	Effect of Pd or Pt addition to Ti/Al ohmic contact materials for n-type AlGaN. Applied Physics Letters, 2002, 80, 2934-2936.	3.3	35
80	Control of normally on/off characteristics in hydrogenated diamond metal-insulator-semiconductor field-effect transistors. Journal of Applied Physics, 2015, 118, .	2.5	35
81	Dependence of electrical properties on work functions of metals contacting to p-type GaN. Applied Surface Science, 1997, 117-118, 373-379.	6.1	33
82	Development of AlN/diamond heterojunction field effect transistors. Diamond and Related Materials, 2012, 24, 206-209.	3.9	31
83	Diamond field effect transistors with a high-dielectric constant Ta ₂ O ₅ as gate material. Journal Physics D: Applied Physics, 2014, 47, 245102.	2.8	31
84	Effects of oxidation conditions on electrical properties of SiC‣iO2interfaces. Journal of Applied Physics, 1990, 68, 6304-6308.	2.5	29
85	Study on determining factors of low contact resistivity in transition metal-silicon systems. Applied Surface Science, 1993, 70-71, 624-628.	6.1	29
86	Sb2O3nanobelt networks for excellent visible-light-range photodetectors. Nanotechnology, 2011, 22, 165704.	2.6	29
87	Diamond logic inverter with enhancement-mode metal-insulator-semiconductor field effect transistor. Applied Physics Letters, 2014, 105, .	3.3	29
88	Large deep-ultraviolet photocurrent in metal-semiconductor-metal structures fabricated on as-grown boron-doped diamond. Applied Physics Letters, 2005, 87, 113507.	3.3	28
89	Electron microscopy studies of the intermediate layers at the SiO ₂ /GaN interface. Japanese Journal of Applied Physics, 2017, 56, 110312.	1.5	28
90	Observation of an ordered structure in the initial stage of Ge/Si heteroepitaxial growth. Applied Physics Letters, 1990, 57, 2434-2436.	3.3	27

#	Article	IF	CITATIONS
91	Energy dissipation in micron- and submicron-thick single crystal diamond mechanical resonators. Applied Physics Letters, 2014, 105, .	3.3	26
92	InGaN-based thin film solar cells: Epitaxy, structural design, and photovoltaic properties. Journal of Applied Physics, 2015, 117, .	2.5	26
93	Assembly of a high-dielectric constant thin TiOx layer directly on H-terminated semiconductor diamond. Applied Physics Letters, 2016, 108, .	3.3	26
94	Improvement of the quality factor of single crystal diamond mechanical resonators. Japanese Journal of Applied Physics, 2017, 56, 024101.	1.5	26
95	Interface trap characterization of Al2O3/GaN vertical-type MOS capacitors on GaN substrate with surface treatments. Journal of Alloys and Compounds, 2018, 767, 600-605.	5.5	26
96	Single-crystal diamond microelectromechanical resonator integrated with a magneto-strictive galfenol film for magnetic sensing. Carbon, 2019, 152, 788-795.	10.3	26
97	Simultaneous observation of luminescence and dissociation processes of Mg–H complex for Mg-doped GaN. Journal of Applied Physics, 2002, 92, 3657-3661.	2.5	25
98	High- <i>k</i> ZrO2/Al2O3 bilayer on hydrogenated diamond: Band configuration, breakdown field, and electrical properties of field-effect transistors. Journal of Applied Physics, 2016, 120, .	2.5	25
99	Ultrahigh Performance Onâ€Chip Single Crystal Diamond NEMS/MEMS with Electrically Tailored Selfâ€Sensing Enhancing Actuation. Advanced Materials Technologies, 2019, 4, 1800325.	5.8	25
100	Photoelectron spectroscopic studies on interfacial reactions in Zr/2×1(100)Si and Zr/SiO2/(100)Si systems. Journal of Vacuum Science and Technology A: Vacuum, Surfaces and Films, 1993, 11, 2619-2622.	2.1	24
101	Development of Pt-based ohmic contact materials for p-type GaN. Journal of Applied Physics, 2001, 89, 2826-2831.	2.5	24
102	Ohmic contact for p-type diamond without postannealing. Journal of Applied Physics, 2008, 104, 016104.	2.5	24
103	Growth mechanism of c-axis-oriented AlN on (0 0 1) diamond substrates by metal-organic vapor phase epitaxy. Journal of Crystal Growth, 2010, 312, 368-372.	1.5	24
104	Effective Use of Source Gas for Diamond Growth with Isotopic Enrichment. Applied Physics Express, 2013, 6, 055601.	2.4	24
105	Enhancing Delta <i>E</i> Effect at High Temperatures of Galfenol/Ti/Single-Crystal Diamond Resonators for Magnetic Sensing. ACS Applied Materials & Interfaces, 2020, 12, 23155-23164.	8.0	24
106	Relationship between growth processes and strain relaxation in Si1â^'xGexfilms grown on (100)Siâ€(2×1) surfaces by gas source molecular beam epitaxy. Journal of Applied Physics, 1993, 73, 2288-2293.	2.5	23
107	Growth mechanism of c-axis-oriented AlN on (1 1 1) diamond substrates by metal-organic vapor phase epitaxy. Journal of Crystal Growth, 2010, 312, 1325-1328.	1.5	23
108	Mechanism of reverse current increase of vertical-type diamond Schottky diodes. Journal of Applied Physics, 2017, 122, .	2.5	23

#	Article	IF	CITATIONS
109	Solid phase reaction and electrical properties in Zr/Si system. Applied Physics Letters, 1990, 57, 1105-1107.	3.3	22
110	Structural properties and transfer characteristics of sputter deposition AlN and atomic layer deposition Al2O3 bilayer gate materials for H-terminated diamond field effect transistors. Journal of Applied Physics, 2016, 120, .	2.5	22
111	Boosting the doping efficiency of Mg in <i>p</i> -GaN grown on the free-standing GaN substrates. Applied Physics Letters, 2019, 115, .	3.3	22
112	Controlled formation of wrinkled diamond-like carbon (DLC) film on grooved poly(dimethylsiloxane) substrate. Diamond and Related Materials, 2012, 22, 48-51.	3.9	21
113	Electrical properties of atomic layer deposited HfO2/Al2O3 multilayer on diamond. Diamond and Related Materials, 2015, 54, 55-58.	3.9	21
114	Comparative Analysis of Defects in Mg-Implanted and Mg-Doped GaN Layers on Freestanding GaN Substrates. Nanoscale Research Letters, 2018, 13, 403.	5.7	21
115	Schottky barrier height and thermal stability of p-diamond (100) Schottky interfaces. Thin Solid Films, 2014, 557, 241-248.	1.8	20
116	Magnetic Control of Magneto-Electrochemical Cell and Electric Double Layer Transistor. Scientific Reports, 2017, 7, 10534.	3.3	20
117	Influence of post-deposition annealing on characteristics of Pt/Al2O3/β-Ga2O3 MOS capacitors. Microelectronic Engineering, 2019, 216, 111040.	2.4	20
118	Diamond Schottky diodes with ideality factors close to 1. Applied Physics Letters, 2014, 105, 133515.	3.3	19
119	Electrical hysteresis in p-GaN metal–oxide–semiconductor capacitor with atomic-layer-deposited Al ₂ O ₃ as gate dielectric. Applied Physics Express, 2016, 9, 121002.	2.4	19
120	Layered boron nitride enabling high-performance AlGaN/GaN high electron mobility transistor. Journal of Alloys and Compounds, 2020, 829, 154542.	5.5	19
121	Coupling of magneto-strictive FeGa film with single-crystal diamond MEMS resonator for high-reliability magnetic sensing at high temperatures. Materials Research Letters, 2020, 8, 180-186.	8.7	19
122	Growth processes in the initial stage of Ge films on (811)Si surfaces by GeH4source molecular beam epitaxy. Journal of Applied Physics, 1990, 68, 2164-2167.	2.5	18
123	In-situ RHEED study of growth processes in the initial stage of SiGe alloy film deposition by gas source molecular beam epitaxy. Journal of Crystal Growth, 1991, 115, 365-370.	1.5	18
124	High-detectivity nanowire photodetectors governed by bulk photocurrent dynamics with thermally stable carbide contacts. Nanotechnology, 2013, 24, 495701.	2.6	18
125	Vertical-Type Ni/GaN UV Photodetectors Fabricated on Free-Standing GaN Substrates. Applied Sciences (Switzerland), 2019, 9, 2895.	2.5	18
126	Enhanced magnetic sensing performance of diamond MEMS magnetic sensor with boron-doped FeGa film. Carbon. 2020. 170. 294-301.	10.3	18

#	Article	IF	CITATIONS
127	Fixed charges investigation in Al2O3/hydrogenated-diamond metal-oxide-semiconductor capacitors. Applied Physics Letters, 2020, 117, .	3.3	18
128	Metal–diamond semiconductor interface and photodiode application. Applied Surface Science, 2008, 254, 6268-6272.	6.1	17
129	Integration of (PbZr0.52Ti0.48O3) on single crystal diamond as metal-ferroelectric-insulator-semiconductor capacitor. Applied Physics Letters, 2009, 94, .	3.3	17
130	Systematic investigation of surface and bulk electronic structure of undoped In-polar InN epilayers by hard X-ray photoelectron spectroscopy. Journal of Applied Physics, 2013, 114, .	2.5	17
131	Suppression in the electrical hysteresis by using CaF2 dielectric layer for p-GaN MIS capacitors. Journal of Applied Physics, 2018, 123, .	2.5	17
132	High Output Current Boron-Doped Diamond Metal-Semiconductor Field-Effect Transistors. IEEE Electron Device Letters, 2019, 40, 1748-1751.	3.9	17
133	Investigation of Al2O3/GaN interface properties by sub-bandgap photo-assisted capacitance-voltage technique. AlP Advances, 2019, 9, .	1.3	17
134	Characteristics of Al ₂ O ₃ /native oxide/n-GaN capacitors by post-metallization annealing. Semiconductor Science and Technology, 2019, 34, 034001.	2.0	17
135	Temperature dependence of Young's modulus of single-crystal diamond determined by dynamic resonance. Diamond and Related Materials, 2021, 116, 108403.	3.9	17
136	Reducing intrinsic energy dissipation in diamond-on-diamond mechanical resonators toward one million quality factor. Physical Review Materials, 2018, 2, .	2.4	17
137	Effects of surface cleaning on electrical properties for Ni contacts to p-type ZnSe. Journal of Vacuum Science & Technology an Official Journal of the American Vacuum Society B, Microelectronics Processing and Phenomena, 1996, 14, 1812.	1.6	16
138	Carrier transport mechanisms through the metal/p-type diamond semiconductor interface. Diamond and Related Materials, 1997, 6, 847-851.	3.9	16
139	pâ€type diamond Schottky diodes fabricated by vacuum ultraviolet light/ozone surface oxidation: Comparison with diodes based on wetâ€chemical oxidation. Physica Status Solidi (A) Applications and Materials Science, 2009, 206, 2082-2085.	1.8	16
140	Impedance analysis of Al2O3/H-terminated diamond metal-oxide-semiconductor structures. Applied Physics Letters, 2015, 106, 083506.	3.3	16
141	Effect of off-cut angle of hydrogen-terminated diamond(111) substrate on the quality of AlN towards high-density AlN/diamond(111) interface hole channel. Journal of Applied Physics, 2017, 121, .	2.5	16
142	Low-energy ion scattering spectroscopy and reflection high-energy electron diffraction of native oxides on GaN(0001). Japanese Journal of Applied Physics, 2017, 56, 128004.	1.5	16
143	Vaporâ€Phase Etching of InP Using Anhydrous HCl and  PH 3 Gas. Journal of the Electrochemical Society, 1986, 133, 2204-2205.	2.9	15
144	Schottky barrier heights of metals contacting to p-ZnSe. Journal of Applied Physics, 1997, 82, 2393-2399.	2.5	15

#	Article	IF	CITATIONS
145	Annealing effects on hydrogenated diamond NOR logic circuits. Applied Physics Letters, 2018, 112, .	3.3	15
146	Effect of Boron Incorporation on Structural and Optical Properties of AlN Layers Grown by Metalâ€Organic Vapor Phase Epitaxy. Physica Status Solidi (A) Applications and Materials Science, 2018, 215, 1800282.	1.8	15
147	The electric double layer effect and its strong suppression at Li+ solid electrolyte/hydrogenated diamond interfaces. Communications Chemistry, 2021, 4, .	4.5	15
148	Formation of a superstructure in the initial stage of Ge epitaxial growth on Si(100) substrates. Applied Surface Science, 1991, 48-49, 69-75.	6.1	14
149	Dependence of Electrical Properties on Work Functions of Metals Contacting to p-type ZnSe. Japanese Journal of Applied Physics, 1996, 35, 1657-1663.	1.5	14
150	Crystallographic and electrical characterization of tungsten carbide thin films for Schottky contact of diamond photodiode. Journal of Vacuum Science & Technology B, 2006, 24, 185.	1.3	14
151	Schottky-barrier photodiode using p-diamond epilayer grown on p+-diamond substrates. Diamond and Related Materials, 2009, 18, 296-298.	3.9	14
152	High-performance visible to near-infrared photodetectors by using (Cd,Zn)Te single crystal. Optics Express, 2019, 27, 8935.	3.4	14
153	Peculiarity of Depletion Region in Diamond pn-Junction. Japanese Journal of Applied Physics, 2003, 42, 6800-6803.	1.5	13
154	Electrical characterization of Schottky diodes based on boron doped homoepitaxial diamond films by conducting probe atomic force microscopy. Superlattices and Microstructures, 2006, 40, 343-349.	3.1	13
155	Submicron metal-semiconductor-metal diamond photodiodes toward improving the responsivity. Applied Physics Letters, 2007, 91, 163510.	3.3	13
156	Chemical Vapor Deposition of ¹² C Isotopically Enriched Polycrystalline Diamond. Japanese Journal of Applied Physics, 2012, 51, 090104.	1.5	13
157	Nanoelectromechanical switch fabricated from single crystal diamond: Experiments and modeling. Diamond and Related Materials, 2012, 24, 69-73.	3.9	13
158	Operations of hydrogenated diamond metal–oxide–semiconductor field-effect transistors after annealing at 500 °C. Journal Physics D: Applied Physics, 2019, 52, 315104.	2.8	13
159	Epitaxial Combination of Two-Dimensional Hexagonal Boron Nitride with Single-Crystalline Diamond Substrate. ACS Applied Materials & Interfaces, 2020, 12, 46466-46475.	8.0	13
160	NiGe-based ohmic contacts to n-type GaAs. Journal of Electronic Materials, 1996, 25, 1684-1694.	2.2	12
161	Electric field breakdown of lateral-type Schottky diodes formed on lightly doped homoepitaxial diamond. Applied Surface Science, 2008, 254, 6273-6276.	6.1	12
162	Schottky photodiode using submicron thick diamond epilayer for flame sensing. Nano-Micro Letters, 2009, 1, 30-33.	27.0	12

#	Article	IF	CITATIONS
163	Improved ferroelectric properties of Pb(Zr0.52,Ti0.48)O3 thin film on single crystal diamond using CaF2 layer. Applied Physics Letters, 2010, 96, .	3.3	12
164	Amorphous silicon diamond based heterojunctions with high rectification ratio. Journal of Non-Crystalline Solids, 2012, 358, 2110-2113.	3.1	12
165	Localized mid-gap-states limited reverse current of diamond Schottky diodes. Journal of Applied Physics, 2012, 111, 104503.	2.5	12
166	Spectrally dependent photovoltages in Schottky photodiode based on (100) B-doped diamond. Journal of Applied Physics, 2014, 115, 053105.	2.5	12
167	An Overview of High-k Oxides on Hydrogenated-Diamond for Metal-Oxide-Semiconductor Capacitors and Field-Effect Transistors. Sensors, 2018, 18, 1813.	3.8	12
168	Yâ€Ba uâ€O superconducting thin films prepared by plasmaâ€assisted flash evaporation. Applied Physics Letters, 1989, 55, 307-309.	3.3	11
169	Formation and deterioration mechanisms of low-resistance TaTi ohmic contacts forp-GaN. Journal of Applied Physics, 1999, 86, 5079-5084.	2.5	11
170	Analysis of Electron Statistics Involving Compensation and Deep-Dopant Effects for Phosphorus-Doped n-Type Diamond. Japanese Journal of Applied Physics, 2004, 43, 3307-3310.	1.5	11
171	Piezoelectric Pb(Zr0.52Ti0.48)O3 thin films on single crystal diamond: Structural, electrical, dielectric, and field-effect-transistor properties. Journal of Applied Physics, 2010, 107, 024101.	2.5	11
172	Interfacial electronic band alignment of Ta2O5/hydrogen-terminated diamond heterojunction determined by X-ray photoelectron spectroscopy. Diamond and Related Materials, 2013, 38, 24-27.	3.9	11
173	Thermal stabilization and deterioration of the WC/pâ€type diamond (100) Schottkyâ€barrier interface. Physica Status Solidi (A) Applications and Materials Science, 2014, 211, 2363-2366.	1.8	11
174	Direct observation of the leakage current in epitaxial diamond Schottky barrier devices by conductive-probe atomic force microscopy and Raman imaging. Journal Physics D: Applied Physics, 2014, 47, 355102.	2.8	11
175	Reducing energy dissipation and surface effect of diamond nanoelectromechanical resonators by annealing in oxygen ambient. Carbon, 2017, 124, 281-287.	10.3	11
176	Characterization of a 4-inch GaN wafer by X-ray diffraction topography. CrystEngComm, 2018, 20, 7761-7765.	2.6	11
177	Lattice-plane orientation mapping of homo-epitaxial GaN(0001) thin films via grazing-incidence X-ray diffraction topography in 2-in. wafer. Applied Physics Express, 2018, 11, 081002.	2.4	11
178	Local photoconductivity on diamond metal-semiconductor-metal photodetectors measured by conducting probe atomic force microscopy. Diamond and Related Materials, 2007, 16, 1074-1077.	3.9	10
179	Effect of Annealing Temperature on Performances of Boron-Doped Diamond Metal–Semiconductor Field-Effect Transistors. IEEE Transactions on Electron Devices, 2020, 67, 1680-1685.	3.0	10
180	Science and Technology of Integrated Super-High Dielectric Constant AlOx/TiOy Nanolaminates / Diamond for MOS Capacitors and MOSFETs. Carbon, 2021, 172, 112-121.	10.3	10

#	Article	IF	CITATIONS
181	Boron-Doped Diamond MOSFETs With High Output Current and Extrinsic Transconductance. IEEE Transactions on Electron Devices, 2021, 68, 3963-3967.	3.0	10
182	Tungsten carbide Schottky contact to diamond toward thermally stable photodiode. Diamond and Related Materials, 2005, 14, 2003-2006.	3.9	9
183	Admittance spectroscopy for phosphorus-doped n-type diamond epilayer. Applied Physics Letters, 2005, 86, 232105.	3.3	9
184	Mechanism of photoconductivity gain and persistent photoconductivity for diamond photodetector. Diamond and Related Materials, 2010, 19, 205-207.	3.9	9
185	Polarization Filters for Visible Light Consisting of Subwavelength Slits in an Aluminum Film. Journal of Lightwave Technology, 2012, 30, 3463-3467.	4.6	9
186	High-quality SiN _{<i>x</i>} / <i>p</i> -GaN metal-insulator-semiconductor interface with low-density trap states. Journal Physics D: Applied Physics, 2019, 52, 085105.	2.8	9
187	Formation of interfacial layers and electrical conduction mechanisms dominating the contact resistivity in refractory metal-Si contacts. Applied Surface Science, 1992, 56-58, 545-550.	6.1	8
188	Cd-based ohmic contact materials to p-ZnSe. Journal of Crystal Growth, 1996, 159, 709-713.	1.5	8
189	Near-noble transition-metal-based ohmic contacts to p-InP: Comparison of Ni and Pd as a base metal. Journal of Applied Physics, 1999, 85, 7792-7796.	2.5	8
190	Impact of Mg concentration on energy-band-depth profile of Mg-doped InN epilayers analyzed by hard X-ray photoelectron spectroscopy. Applied Physics Letters, 2013, 103, .	3.3	8
191	Temperature and Light Intensity Dependence of Photocurrent Transport Mechanisms in InGaN p–i–n Homojunction Solar Cells. Japanese Journal of Applied Physics, 2013, 52, 08JF04.	1.5	8
192	Self-assembling diacetylene molecules on atomically flat insulators. Physical Chemistry Chemical Physics, 2016, 18, 31600-31605.	2.8	8
193	Homoepitaxial diamond chemical vapor deposition for ultra-light doping. Materials Science in Semiconductor Processing, 2017, 70, 197-202.	4.0	8
194	A density functional study of the effect of hydrogen on electronic properties and band discontinuity at anatase TiO2/diamond interface. Journal of Applied Physics, 2018, 123, .	2.5	8
195	Synchrotron X-ray diffraction characterization of the inheritance of GaN homoepitaxial thin films grown on selective growth substrates. CrystEngComm, 2018, 20, 2861-2867.	2.6	8
196	Electron microscopy and ultraviolet photoemission spectroscopy studies of native oxides on GaN(0001). Japanese Journal of Applied Physics, 2018, 57, 098003.	1.5	8
197	Formation of Si-SiO2 interfaces at low temperatures using microwave-excited plasma. Applied Surface Science, 1990, 41-42, 429-432.	6.1	7
198	Initial growth of Ge films on Si(111)7 × 7 surfaces by gas source molecular beam epitaxy. Applied Surface Science, 1992, 60-61, 120-125.	6.1	7

#	Article	IF	CITATIONS
199	Effects of Small Amounts of Silver Added to NiGe Ohmic Contacts to nâ€Type GaAs. Journal of the Electrochemical Society, 1996, 143, 1705-1709.	2.9	7
200	The effect of a thin antimony layer addition on PdZn ohmic contacts for p-type InP. Applied Surface Science, 2000, 159-160, 174-178.	6.1	7
201	Vertical-type Schottky-barrier photodiode using p-diamond epilayer grown on heavily boron-doped p+-diamond substrate. Diamond and Related Materials, 2008, 17, 1916-1921.	3.9	7
202	Microstructure of AlN with two-domain structure on (001) diamond substrate grown by metal-organic vapor phase epitaxy. Diamond and Related Materials, 2010, 19, 131-133.	3.9	7
203	Interfacial chemical bonding state and band alignment of CaF2/hydrogen-terminated diamond heterojunction. Journal of Applied Physics, 2013, 113, 123706.	2.5	7
204	Investigation on the interfacial chemical state and band alignment for the sputtering-deposited CaF2/ <i>p</i> -GaN heterojunction by angle-resolved X-ray photoelectron spectroscopy. Journal of Applied Physics, 2016, 120, .	2.5	7
205	Surface potential imaging and characterizations of a GaN p-n junction with Kelvin probe force microscopy. AIP Advances, 2020, 10, .	1.3	7
206	Interface characteristics of β-Ga2O3/Al2O3/Pt capacitors after postmetallization annealing. Journal of Vacuum Science and Technology A: Vacuum, Surfaces and Films, 2021, 39, .	2.1	7
207	Atomic mixing phenomena and changes in faceted structure of Ge films grown on (100)Si by thermal annealing. Journal of Crystal Growth, 1991, 115, 106-111.	1.5	6
208	Effect of the first antimony layer on AuZn ohmic contacts to p-type InP. Journal of Vacuum Science & Technology an Official Journal of the American Vacuum Society B, Microelectronics Processing and Phenomena, 2000, 18, 1957.	1.6	6
209	CoAl Ohmic Contact Materials with Improved Surface Morphology for p-Type 4H-SiC. Materials Science Forum, 2002, 389-393, 885-888.	0.3	6
210	Development of Thermally Stable, Solar-Blind Deep-Ultraviolet Diamond Photosensor. Materials Transactions, 2005, 46, 1965-1968.	1.2	6
211	Ultraviolet Detectors Based on Ultraviolet–Ozone Modified Hydrogenated Diamond Surfaces. Applied Physics Express, 0, 2, 065501.	2.4	6
212	RGB color filter comprising aluminum film with surface plasmon enhanced transmission through sub-wavelength hole-arrays. , 2009, , .		6
213	Thermal stability investigation for Ohmic contact properties of Pt, Au, and Pd electrodes on the same hydrogen-terminated diamond. AIP Advances, 2020, 10, .	1.3	6
214	Precise characterization of atomic-scale corrosion of single crystal diamond in H2 plasma based on MEMS/NEMS. Corrosion Science, 2020, 170, 108651.	6.6	6
215	Polarization-induced hole doping for long-wavelength In-rich InGaN solar cells. Applied Physics Letters, 2021, 119, .	3.3	6
216	Behaviour of Zn as dopant in the photoluminescence of AlxGa1-xN. Solid State Communications, 1986, 57, 17-20.	1.9	5

#	Article	IF	CITATIONS
217	Anisotropy of piezoresistance in nâ€channel inversion layers of metalâ€oxideâ€semiconductor transistors on (001)Si. Journal of Applied Physics, 1990, 68, 5687-5691.	2.5	5
218	Cd and Te-based ohmic contact materials to p-Type ZnSe. Journal of Electronic Materials, 1996, 25, 1823-1831.	2.2	5
219	Field emission of polycrystalline diamond films grown by microwave plasma chemical vapor deposition. II. Effect of p-type doping in diamond. Diamond and Related Materials, 2001, 10, 2118-2124.	3.9	5
220	Field emission of polycrystalline diamond films grown by microwave-plasma chemical vapor deposition. I. Effects of surface morphology of diamond. Diamond and Related Materials, 2002, 11, 1897-1904.	3.9	5
221	Influence of oxygen on luminescence and vibrational spectra of Mg-doped GaN. Physica Status Solidi (B): Basic Research, 2003, 240, 356-359.	1.5	5
222	Color Filter Based on Surface Plasmon Resonance Utilizing Sub-Micron Periodic Hole Array in Aluminum Thin Film. IEICE Transactions on Electronics, 2012, E95-C, 251-254.	0.6	5
223	Analysis of Broken Symmetry in Convergent-Beam Electron Diffraction along <112̄0 > and <11̄00 > Zone-Axes of AlN for Polarity Determination. Japanese Journal of Applied Physics, 2013, 52, 08JE15.	1.5	5
224	Surface and bulk electronic structures of heavily Mg-doped InN epilayer by hard X-ray photoelectron spectroscopy. Journal of Applied Physics, 2017, 121, .	2.5	5
225	Fabrication of Hydrogenated Diamond Metal–Insulator–Semiconductor Field-Effect Transistors. Methods in Molecular Biology, 2017, 1572, 217-232.	0.9	5
226	Nanometer-thin ALD-Al ₂ O ₃ for the improvement of the structural quality of AlN grown on sapphire substrate by MOVPE. Physica Status Solidi (A) Applications and Materials Science, 2017, 214, 1600727.	1.8	5
227	Investigation of intermediate layers in oxides/GaN(0001) by electron microscopy. Japanese Journal of Applied Physics, 2018, 57, 118003.	1.5	5
228	Evaluation of lattice curvature and crystalline homogeneity for 2-inch GaN homo-epitaxial layer. AIP Advances, 2018, 8, .	1.3	5
229	Anisotropic mosaicity and lattice-plane twisting of an <i>m</i> -plane GaN homoepitaxial layer. CrystEngComm, 2019, 21, 4036-4041.	2.6	5
230	Hydrogen effect on Pt/Al2O3/GaN metal-oxide-semiconductor capacitors. Japanese Journal of Applied Physics, 2019, 58, 100915.	1.5	5
231	Mapping of a Lattice-Plane Tilting in a <mml:math <br="" xmlns:mml="http://www.w3.org/1998/Math/MathML">display="inline" overflow="scroll"><mml:mrow><mml:mi>Ga</mml:mi><mml:mi mathvariant="normal">N</mml:mi </mml:mrow></mml:math> Wafer Using Energy-Resolved X-Ray Diffraction Topography. Physical Review Applied. 2019. 11	3.8	5
232	Suppression of the regrowth interface leakage current in AlGaN/GaN HEMTs by unactivated Mg doped GaN layer. Applied Physics Letters, 2021, 118, 072103.	3.3	5
233	Stress effect on the resonance properties of single-crystal diamond cantilever resonators for microscopy applications. Ultramicroscopy, 2022, 234, 113464.	1.9	5
234	Depletion layer in pn-junction of diamond with phosphorus donor and boron acceptor. Diamond and Related Materials, 2004, 13, 1963-1966.	3.9	4

#	Article	IF	CITATIONS
235	Mechanism of photoconductivity gain for p-diamond Schottky photodiode. Diamond and Related Materials, 2007, 16, 949-952.	3.9	4
236	Influence of surface structure of (0001) sapphire substrate on the elimination of small-angle grain boundary in AlN epilayer. AIP Advances, 2015, 5, 097143.	1.3	4
237	Lattice-plane bending angle modulation of Mg-doped GaN homoepitaxial layer observed by X-ray diffraction topography. CrystEngComm, 2019, 21, 2281-2285.	2.6	4
238	Highly-crystalline 6 inch free-standing GaN observed using X-ray diffraction topography. CrystEngComm, 2021, 23, 1628-1633.	2.6	4
239	Admittance spectroscopy of a phosphorus-doped n-diamond homoepitaxial layer. Diamond and Related Materials, 2005, 14, 2011-2014.	3.9	3
240	Analysis of polar direction of AlN grown on (0001) sapphire and 6Hâ€SiC substrates by highâ€ŧemperature metalâ€organic vapor phase epitaxy using coaxial impact collision ion scattering spectroscopy. Physica Status Solidi C: Current Topics in Solid State Physics, 2010, 7, 2365-2367.	0.8	3
241	Fabrication and electrical properties of SrTiO3/diamond junctions. Diamond and Related Materials, 2010, 19, 319-323.	3.9	3
242	Influence of post-deposition annealing on interface characteristics at Al ₂ O ₃ /n-GaN. , 2019, , .		3
243	High Current Output Hydrogenated Diamond Triple-Gate MOSFETs. IEEE Journal of the Electron Devices Society, 2019, 7, 561-565.	2.1	3
244	Surface morphology smoothing of a 2 inch-diameter GaN homoepitaxial layer observed by X-ray diffraction topography. RSC Advances, 2020, 10, 1878-1882.	3.6	3
245	Thermal mismatch induced stress characterization by dynamic resonance based on diamond MEMS. Applied Physics Express, 2021, 14, 045501.	2.4	3
246	Investigation of Ohmic Contact Resistance, Surface Resistance, and Channel Resistance for Hydrogen-Terminated Diamond MOSFETs. IEEE Transactions on Electron Devices, 2022, 69, 1181-1185.	3.0	3
247	Enhancement of donor ionization in phosphorus-doped n-diamond. Applied Surface Science, 2005, 244, 26-29.	6.1	2
248	Simulation of Band Diagram for Chemical-Vapor-Deposition Diamond Surface Conductivity. Japanese Journal of Applied Physics, 2005, 44, 8378-8382.	1.5	2
249	Effects of shallow traps on the reverse current of diamond Schottky diode: An electrical transient study. Physica Status Solidi (A) Applications and Materials Science, 2010, 207, 1460-1463.	1.8	2
250	InGaN photodiodes using CaF2 insulator for high-temperature UV detection. Physica Status Solidi C: Current Topics in Solid State Physics, 2012, 9, 953-956.	0.8	2
251	Single Crystal Diamond Micromechanical and Nanomechanical Resonators. Topics in Applied Physics, 2019, , 91-121.	0.8	2
252	<i>(Invited) </i> Characteristics of Several High-k Gate Insulators for GaN Power Device. ECS Transactions, 2019, 92, 109-117.	0.5	2

#	Article	IF	CITATIONS
253	Threshold Voltage Instability of Diamond Metal–Oxide–Semiconductor Fieldâ€Effect Transistors Based on 2D Hole Gas. Physica Status Solidi (A) Applications and Materials Science, 2019, 216, 1900538.	1.8	2
254	Electrical readout/characterization of single crystal diamond (SCD) cantilever resonators. Diamond and Related Materials, 2020, 103, 107711.	3.9	2
255	Integrated TbDyFe Film on a Singleâ€Crystal Diamond Microelectromechanical Resonator for Magnetic Sensing. Physica Status Solidi - Rapid Research Letters, 2021, 15, 2100352.	2.4	2
256	Influence of HfO2 and SiO2 interfacial layers on the characteristics of n-GaN/HfSiO <i>x</i> capacitors using plasma-enhanced atomic layer deposition. Journal of Vacuum Science and Technology A: Vacuum, Surfaces and Films, 2021, 39, .	2.1	2
257	In-situ RHEED study on the effect of light irradiation on Ge/Si heteroepitaxial growth by GeH4 source MBE. Journal of Crystal Growth, 1992, 120, 284-289.	1.5	1
258	Observation of SiSiO2 interface states within the conduction band by tunneling current spectroscopy. Applied Surface Science, 1992, 56-58, 841-845.	6.1	1
259	RHEED studies of initial stage of Ge film growth on (311)Si by gas source molecular beam epitaxy. Journal of Crystal Growth, 1993, 128, 319-326.	1.5	1
260	Photo-irradiation effects on surface reactions in Si monolayer overgrowth by Si2H6 source MBE. Applied Surface Science, 1994, 79-80, 304-309.	6.1	1
261	Schottky barrier heights of contact metals to p-type ZnSe. Journal of Electronic Materials, 1998, 27, 772-775.	2.2	1
262	Electrical properties at p-ZnSe/metal interfaces. Journal of Electronic Materials, 1998, 27, 929-935.	2.2	1
263	Ohmic contacts to p-ZnSe and p-GaN wide-gap semiconductors. Electronics and Communications in Japan, 1999, 82, 43-47.	0.2	1
264	Evolution of nanophotonics from semiconductor photonic crystal device to metal/semiconductor plasmonic device. , 2010, , .		1
265	Photodetectors: Flexible Ultraviolet Photodetectors with Broad Photoresponse Based on Branched ZnS-ZnO Heterostructure Nanofilms (Adv. Mater. 19/2014). Advanced Materials, 2014, 26, 3087-3087.	21.0	1
266	Displacement current of Au/p-diamond Schottky contacts. Materials Science in Semiconductor Processing, 2017, 70, 207-212.	4.0	1
267	Effect of Sputter Deposition Atmosphere of AlN on the Electrical Properties of Hydrogenâ€Terminated Diamond Field Effect Transistor with AlN/Al ₂ O ₃ Stack Gate. Physica Status Solidi (A) Applications and Materials Science, 2017, 214, 1700463.	1.8	1
268	Surface and bulk electronic structures of unintentionally and Mg-doped In0.7Ga0.3N epilayer by hard X-ray photoelectron spectroscopy. Journal of Applied Physics, 2018, 123, 095701.	2.5	1
269	Optical Filters Based on Nano-Sized Hole and Slit Patterns in Aluminum Films. IEICE Transactions on Electronics, 2016, E99.C, 358-364.	0.6	1
270	Current Progress of Pressure Sensors for Harsh Environments Based on Wide-Bandgap Semiconductors. Recent Patents on Materials Science, 2010, 3, 96-105.	0.5	1

#	Article	IF	CITATIONS
271	High-spatial resolution analysis of interfaces of semiconductor superlattices by using nm-sized electron probe. , 1994, , 315-320.		1
272	Effects of intermediate semiconductor layers on carrier transport mechanisms through p-ZnSe/metals interfaces. Journal of Electronic Materials, 1998, 27, 998-1002.	2.2	0
273	Theoretical Analysis of Electron Statistics for n-Type Diamond. Materials Science Forum, 2005, 475-479, 1719-1724.	0.3	0
274	Development of Electrode Materials for Semiconductor Devices. Materials Science Forum, 2005, 475-479, 1705-1714.	0.3	0
275	Analysis for Electron Concentrations in n-Diamond/III–Nitride Heterostructure and Phosphorus δ-Doped Structure in Diamond. Japanese Journal of Applied Physics, 2005, 44, 55-59.	1.5	0
276	Visible-Blind Metal-Semiconductor-Metal Structured Deep-Ultraviolet Photodetectors Using Single-Crystalline Diamond Thin Film. Materials Science Forum, 2007, 546-549, 1759-1762.	0.3	0
277	Nanophotonics technology for advanced quantum dot/photonic crystal device and metal/semiconductor plasmonic device. , 2010, , .		0
278	Nanoelectromechanical switches based on diamond-on-diamond. , 2011, , .		0
279	Bridging wide bandgap nanowires for ultraviolet light detection. , 2011, , .		0
280	Diamond FETs using heterojunction and high-k dielectrics. , 2014, , .		0
281	Formation Mechanism and Elimination of Smallâ€Angle Grain Boundary in AlN Grown on (0001) Sapphire Substrate. , 2017, , .		0
282	High-k Oxides on Hydrogenated-Diamond for Metal-Oxide-Semiconductor Field-Effect Transistors [Invited]. , 2019, , .		0
283	⁷¹ Ga NMR characterization of an n-doped free-standing gallium nitride wafer. Japanese Journal of Applied Physics, 2019, 58, 031003.	1.5	0
284	Reliable Ohmic Contact Properties for Ni/Hydrogen-Terminated Diamond at Annealing Temperature up to 900 °C. Coatings, 2021, 11, 470.	2.6	0
285	Ambient-hydrogen-induced changes in the characteristics of Pt/GaN Schottky diodes fabricated on bulk GaN substrates. Japanese Journal of Applied Physics, 2021, 60, 068003.	1.5	0
286	Current Progress of Pressure Sensors for Harsh Environments Based on Wide-Bandgap Semiconductors. Recent Patents on Materials Science, 2010, 3, 96-105.	0.5	0
287	Nanophotonics Based on Semiconductor-Photonic Crystal/Quantum Dot and Metal-/Semiconductor-Plasmonics. IEICE Transactions on Electronics, 2012, E95-C, 178-187.	0.6	0
288	Development of Diamond-based Optical and Electronic Devices. Journal of Smart Processing, 2013, 2, 224-229.	0.1	0

#	Article	IF	CITATIONS
289	Microstructural Analysis at Metal/Semiconductor Interface for Ideal Ohmic Contacts. Materia Japan, 1998, 37, 998-998.	0.1	0
290	Crystalline Diamond Substrates for Power Devices. Journal of the Institute of Electrical Engineers of Japan, 2017, 137, 689-692.	0.0	0
291	Study of HfSiO _x film as gate insulator for GaN power device. , 2021, , .		0
292	Improvement of structural quality of AIN layers grown on c-plane sapphire substrate by metal–organic vapor phase epitaxy using post-growth annealing with trimethylgallium. AIP Advances, 2022, 12, 015203.	1.3	0
293	Schottky photodiode using submicron thick diamond epilayer for flame sensing. Nano-Micro Letters, 2010, 1, .	27.0	0